Article

# Dual-Mode Fluorophore-Doped Nickel Nitrilotriacetic Acid-Modified Silica Nanoparticles Combine Histidine-Tagged Protein Purification with Site-Specific Fluorophore Labeling

Sung Hoon Kim, M. Jeyakumar, and John A. Katzenellenbogen

*J. Am. Chem. Soc.*, **2007**, 129 (43), 13254-13264• DOI: 10.1021/ja074443f • Publication Date (Web): 02 October 2007



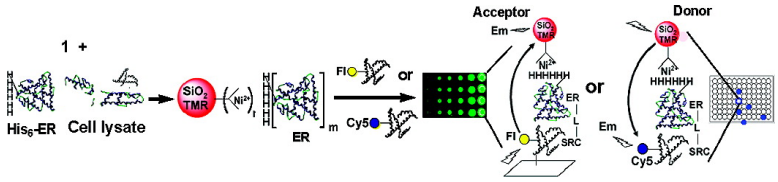


## More About This Article

Additional resources and features associated with this article are available within the HTML version:

- Supporting Information
- Links to the 6 articles that cite this article, as of the time of this article download
- Access to high resolution figures
- Links to articles and content related to this article
- Copyright permission to reproduce figures and/or text from this article

View the Full Text HTML

J|A|C|S
ARTICLES
Published on Web 10/02/2007

# Dual-Mode Fluorophore-Doped Nickel Nitrilotriacetic Acid-Modified Silica Nanoparticles Combine Histidine-Tagged Protein Purification with Site-Specific Fluorophore Labeling

Sung Hoon Kim, M. Jeyakumar, and John A. Katzenellenbogen*

*Contribution from the Department of Chemistry, University of Illinois, 600 South Mathews Avenue, Urbana, Illinois 61801*

Received July 2, 2007; E-mail: jkatzene@uiuc.edu

***Abstract:*** We present the first example of a fluorophore-doped nickel chelate surface-modified silica nanoparticle that functions in a dual mode, combining histidine-tagged protein purification with site-specific fluorophore labeling. Tetramethylrhodamine (TMR)-doped silica nanoparticles, estimated to contain 700−900 TMRs per ca. 23 nm particle, were surface modified with nitrilotriacetic acid (NTA), producing TMR-$SiO_2$-NTA-$Ni^{2+}$. Silica-embedded TMR retains very high quantum yield, is resistant to quenching by buffer components, and is modestly quenched and only to a certain depth (ca. 2 nm) by surface-attached $Ni^{2+}$. When exposed to a bacterial lysate containing estrogen receptor α ligand binding domain (ERα) as a minor component, these beads showed very high specificity binding, enabling protein purification in one step. The capacity and specificity of these beads for binding a his-tagged protein were characterized by electrophoresis, radiometric counting, and MALDI-TOF MS. ERα, bound to TMR-$SiO_2$-NTA-$Ni^{++}$ beads in a site-specific manner, exhibited good activity for ligand binding and for ligand-induced binding to coactivators in solution FRET experiments and protein microarray fluorometric and FRET assays. This dual-mode type TMR-$SiO_2$-NTA-$Ni^{2+}$ system represents a powerful combination of one-step histidine-tagged protein purification and site-specific labeling with multiple fluorophore species.

## 1. Introduction

In the post-proteomics era, a variety of technologies have emerged to assist in profiling cellular proteins and assigning their functions. Prominent among these are fluorescence-based methods, such as fluorescence resonance energy transfer (FRET),[1,2] used both in cells and in high throughput screening with purified proteins to characterize and quantify protein−protein, protein−gene, and protein−ligand interactions.

Three factors need to be considered in the development of effective fluorometric and FRET assays methods. First, it is important to have photostable fluorophores to get reliable fluorescence data that can be related quantitatively to various types of interactions (e.g., protein−protein, protein−gene, and protein−ligand), information that is often important for drug design. Frequently, however, the organic dyes or green fluorescent protein (GFP) suffer from quenching and photobleaching.[3] Also, although FRET assays in cells using GFP can provide very useful information, they require the protein of interest to be genetically fused to the fluorescent proteins. Alternative modes for protein-fluorophore labeling involve genetic modifications to make them selectively reactive with certain fluorophore derivatives (FlAsH and ReAsH technology).[4] Inorganic quantum dots, despite their excellent brightness, are inherently hydrophobic and require derivatization to make them more biocompatible.[5] In addition, they often exhibit stochastic blinking as single emitters, and their brightness in biological matrices can be reduced.[6]

Second, it is often desirable to achieve site-specific conjugation of the fluorophore to a target protein, as well as to effect purification of the fluorophore-labeled protein by methods that can furnish it the high concentration useful for setting up high throughput assays. Third, it can also be helpful to have the fluorophores involved in a FRET assay be relatively rigid, so that FRET data can be related to the distance between the fluorophores. This is more difficult to achieve when the fluorophores have dynamic character by being linked to their interacting elements with flexible tethers. Even tethering one of the two fluorophores involved in FRET can improve distance estimates. If fluorophores are embedded inside of a particle and the surface of the particle is properly modified to capture a target protein, one might expect that protein flexibility and dynamic motion of this dye will be reduced; sensitivity might also be increased, as well, if multiple fluorophores can be engaged per protein. We have considered these three issues in our adaptation of a nanoparticle system for fluorometry and FRET in which the fluorophore is well encapsulated within the particle and the

(1) Vogel, S. S.; Thaler, C.; Koushik, S. V. *Sci. STKE* **2006**, *2006*, re2.
(2) Giepmans, B. N.; Adams, S. R.; Ellisman, M. H.; Tsien, R. Y. *Science* **2006**, *312*, 217−24.
(3) Tsien, R. Y. *Annu. Rev. Biochem.* **1998**, *67*, 509−44.
(4) Chen, I.; Ting, A. Y. *Curr. Opin. Biotechnol.* **2005**, *16*, 35−40.
(5) Medintz, I. L.; Uyeda, H. T.; Goldman, E. R.; Mattoussi, H. *Nat. Mater.* **2005**, *4*, 435−46.
(6) Yao, J.; Larson, D. R.; Vishwasrao, H. D.; Zipfel, W. R.; Webb, W. W. *Proc. Natl. Acad. Sci. U.S.A.* **2005**, *102*, 14284−9.


**10.1021/ja074443f CCC: $37.00** 

particle surface is suitably functionalized to anchor and purify a target protein.

Recently, dye-doped silica nanospheres[7−9] have been used for cellular imaging[9−11] because of their biocompatibility, ease of synthesis and surface modification, dispersability in water and/or organic solvents, size tunability, and ease of manipulation. Furthermore, their optical brightness and photophysical properties are superior as compared to the free dye and are comparable to those of quantum dots.[10,11] Therefore, we choose dye-doped silica nanoparticles as fluorophores due to their excellent properties. In addition, we considered how the fluorophore-doped silica nanoparticles could be used to achieve protein purification and site-specific fluorophore labeling in one step.

The oligohistidine affinity tag (his-tag) is widely used for the purification of his-tagged protein over nickel nitrilotriacetic acid (Ni-NTA) beads,[12] and affinity labeling of his-tagged proteins with a fluorophore-conjugated NTA system (note, a small molecule, not a nanoparticle) has been reported to give proteins that retain their activity and can be used in FRET assays. The Ebright group used a Cy5-NTA system to label $His_6$-tagged protein site specifically and obtained good results from fluorescence anisotropy measurements and FRET experiments.[13] Recently, the Piehler group reported on a higher affinity fluorophore-conjugated multi-NTA system to label his-tagged proteins,[14,15] but they found that the nickel exerted a quenching effect, reducing the emission intensity of the fluorophores on both histidine tag and some sites on the protein. In fact, this quenching effect was used to monitor protein interactions. In this flexible system, however, these investigators were unable to determine the quenching distance or area caused by the nickel ion. As will be discussed below, we believe that the fluorophores entrapped within the matrix of the silica nanoparticles might be less affected by external nickel ions and thus better able to engage in energy-transfer processes.

In this work, we describe the preparation and characterization of tetramethylrhodamine (TMR)-embedded silica nanoparticles and their elaboration with nickel-NTA surface functionality. These well-defined TMR-doped Ni-NTA surface-modified silica nanoparticles provide a versatile and convenient platform of dual-mode agents, combining histidine-tagged protein solid-phase purification with fluorophore conjugation site specifically at the histidine-tagged region in one step. We also demonstrate the use of these nanoparticles in fluorometric and FRET assay applications, and we show that the TMR fluorophore can act as a donor to Cy5 in a solution FRET assay or as an acceptor from fluorescein in a protein microarray assay system for ligand-dependent protein interactions between the estrogen receptor alpha (ERα) and a steroid receptor coactivator (SRC1) receptor interaction domain. In further investigations, the fluorescence characteristics of the silica embedded TMR have been characterized quantitatively and the effect of nickel quenching has been assessed. To the best of our knowledge, dual-mode dye-doped Ni-NTA-conjugated silica nanoparticles have not been investigated for combined one-step protein affinity purification and site-specific fluorophore tagging.

## 2. Experimental Section

**Materials and Methods.** $^1$H NMR and $^{13}$C NMR spectra were recorded on a Varian Inova-500 at 126 MHz with $CD_2Cl_2$. MALDI-TOF (matrix assisted laser desorption ionization-time of flight) mass analysis (2,5-dihydroxybenzoic acid, DHB, as a matrix) and electrospray ionization mass spectra were obtained using Voyager-DE STR and a Q-TOF Ultima API (Waters Co. Ltd.), respectively. IR (infrared) spectra were obtained by using a Spectrum Bx FT-IR system with 633 nm (He−Ne laser) and Spectrum v2.0 software (Perkin-Elmer). UV absorption spectrum was measured by using an 8451A diode array spectrophotometer (Perkin-Elmer), and the sample was placed in a 1 cm quartz corvette. Fluorescence experiments used a Spex Fluorolog II (model IIIc) cuvette-based fluorometer with Data Max 2.2 software (Spex Industries, Edison, NJ). All data were analyzed with Origin 7.5 (OriginLab Co., MA). TEM (transmission electron microscopy) images were obtained by using a Philips CM200 transmission electron microscope at 120 kV (FEI Co., Hillsboro, OR), and pictures were taken using a TVIPS 2K × 2K digital camera. Samples were mounted over carbon-stabilized Formvar coated 250 mesh Cu grids. X-ray photoelectron spectroscopic spectra (XPS) were taken with a Kratos Axis ULTRA instrument equipped with lens mode (2 mm aperture for low magnification with 0.2 mm diameter analysis area), monochromatic Al 225w (15 mA, 15 kV) for source, 160 eV pass energy for low resolution, and 40 eV pass energy for high resolution.

Compounds and materials were obtained from the sources indicated: radiolabeled estradiol ([$^3$H]estradiol) ([6,7-$^3$H]estra-1,3,5(10)-triene-3,17$\beta$-diol, 50−54 Ci/mmol), *trans*-hydroxytamoxifen (TOT), unlabeled estradiol, 30% bovine serum albumin (BSA) solution, α-benzyloxycarbonyl-lysine, and MOPS (3-[*N*-morpholino]propanesulfonic acid), TFA, 28% $NH_4OH$, and TEOS (tetraethyl orthosilicate) (Sigma Aldrich Chemical Co., St. Louis, MO); ICI164,384 (Tocris Cookson, Ellisville, MO), 3-isocyanatopropyl(trimethoxy)silane, 2-[methoxy(polyethylenoxy)$_{6-9}$propyl]trimethoxysilane (Gelest Inc., Morrisville, PA), tetramethylrhodamine-5-NHS ester (TMR-NHS) (Berry & associates, Inc., MO). (Fluorescein)-NH-MGHHHHHHS-COOH, Cy5 labeled SRC1 NR box II peptide (Cy5-NH-LTERHKILHRLLQEGSPSD-COOH) and Cy5 labeled His6-GG-$NH_2$ (HHHHHHGG-Cy5) were synthesized by the Carver Biotechnology Center at University of Illinois at Urbana−Champaign. $N^{\alpha}$,$N^{\alpha}$-Bis[carboxymethyl]-L-lysine (NTA) was synthesized according to the literature.[16]

**Preparation for Various Silica Nanoparticles To Produce $SiO_2$-TMR-PEG-NTA. (A) Preparation of TMR-Doped Silica Nanoparticles ($SiO_2$-TMR).** To the solution of TMR-NHS (10.5 mg, 0.02 mmol) in 0.4 mL of dried DMF was added 3-aminopropyl(trimethoxy)silane (21.4 mg, 0.12 mmol) by syringe. The reaction proceeded at room temperature, and when TLC analysis showed that the TMR-NHS had disappeared, it was precipitated by adding diethyl ether, washed with THF twice to remove a liberated *N*-hydroxysucicimide and excess 3-aminopropyl(trimethoxy)silane, and dried under vacuum. It was dissolved with ethanol (10.4 mL) and hydrolyzed by the addition of aqueous ammonium hydroxide (28%, 200 $\mu$L) for 8 h. To the separately prepared triethyl orthosilicate (TEOS) (0.476 mL, 2.0 mmol) solution in 50 mL of EtOH containing ammonium hydroxide (28% 1.76 mL) was added 1 mL of the prehydrolyzed TMR-silyl solution by syringe. Reaction was continued for 14 h at 50 °C in a clean 50-mL plastic conical bottle. Particles were collected as follows: The TMR-doped

(7) Van Blaaderen, A.; Vrij, A. *Langmuir* **1992**, *8*, 2921−31.
(8) Ow, H.; Larson, D. R.; Srivastava, M.; Baird, B. A.; Webb, W. W.; Wiesner, U. *Nano Lett.* **2005**, *5*, 113−7.
(9) Tan, W.; Wang, K.; He, X.; Zhao, X. J.; Drake, T.; Wang, L.; Bagwe, R. P. *Med. Res. Rev.* **2004**, *24*, 621−638.
(10) Lin, Y. S.; Tsai, C. P.; Huang, H. Y.; Kuo, C. T.; Hung, Y.; Huang, D. M.; Chen, Y. C.; Mou, C. Y. *Chem. Mater.* **2005**, *17*, 4570−4573.
(11) Burns, A.; Ow, H.; Wiesner, U. *Chem. Soc. Rev.* **2006**, *35*, 1028−42.
(12) Hochuli, E.; Dobeli, H.; Schacher, A. *J. Chromatogr.* **1987**, *411*, 177−84.
(13) Kapanidis, A. N.; Ebright, Y. W.; Ebright, R. H. *J. Am. Chem. Soc.* **2001**, *123*, 12123−12125.
(14) Lata, S.; Gavutis, M.; Tampe, R.; Piehler, J. *J. Am. Chem. Soc.* **2006**, *128*, 2365−72.
(15) Lata, S.; Reichel, A.; Brock, R.; Tampe, R.; Piehler, J. *J. Am. Chem. Soc.* **2005**, *127*, 10205−10215.
(16) Schmitt, L.; Dietrich, C.; Tampe, R. *J. Am. Chem. Soc.* **1994**, *116*, 8485−91.

silica particles were collected by centrifuging at 2000 rpm (220*g*) using a 30K cutoff Amicon membrane tube (Waters Co.). The particles were washed with ethanol (twice) containing 5% ammonium hydroxide solution. Particles were stored in this same solution (4 mg/1 mL EtOH) for the next modification. Finally, dried $SiO_2$-TMR particles were obtained by lyophilization as a deep scarlet powder. See IR spectrum (Figure S1), color photograph of water-dispersed particles (Figure S2), and XPS (Figure S6).

**(B) Preparation of $\omega$-(3-{Trimethoxysilylpropyl}aminocarbonyl)-N$^{\alpha}$,N$^{\alpha}$-bis(carboxymethyl)-lysine *t*-Butyl Ester.** To the solution of N$^{\alpha}$,N$^{\alpha}$-bis(*t*-butoxycarbonyl-methyl)-lysine *t*-butyl ester (86.0 mg, 0.2 mmol) in 0.2 mL of $CD_2Cl_2$ was added 3-cyanatopropyltrimethoxysilane (41 mg, 0.2 mmol) at room temperature. After 20 min, proton and carbon-13 NMR spectra were taken to monitor the reaction. $^1$H NMR ($CD_2Cl_2$, 500 MHz) $\delta$ 0.58 (t, 2H, $J$ = 8.0 Hz), 1.42 (s, 27H), 1.44−1.63 (m, 6H), 3.05−3.13 (m, 4H), 3.27 (t, 1H, $J$ = 7.0 Hz), 3.38 (dd, 4H, $J$ = 8.0, 12.5 Hz), 3.50 (s, 9H), 537 (s, 1H, NH), 5.45 (s, 1H, NH); $^{13}$C NMR ($CD_2Cl_2$, 126 MHz) $\delta$ 6.50, 23.09, 23.90, 28.02, 28.10, 29.51, 30.06, 39.92, 42.88, 50.42, 53.80, 65.16, 80.80, 81.03, 158.96, 170.94, 172.41; HRMS (ESI) *m*/*z* calcd for $C_{29}H_{58}O_{10}N_3Si$ ($M^+$) 636.3891, found 636.3909.

**(C) Deprotection of $\omega$-(3-{Trimethoxysilylpropyl}aminocarbonyl)-N$^{\alpha}$,N$^{\alpha}$-bis(*t*-butoxy-carbonyl-methyl)-lysine *t*-Butyl Ester.** To this mixture solution were added dichloromethane (890 $\mu$L), TFA (452 $\mu$L), and thioanisole (368 $\mu$L), and the mixture was continuously stirred for 4 h at room temperature. Ether (10 mL) was poured into the reaction mixture to cause precipitation. The precipitate was suspended in ether again and recollected. This procedure was repeated twice to remove TFA, and the material obtained was used without further characterization.

**(D) Preparation of $SiO_2$-TMR-NTA Particles.** The stock solution of 5.5 mL was diluted with 5.5 mL of DI water. To this solution was added $\omega$-(3-{trimethoxysilylpropyl}aminocarbonyl)-$N^{\alpha}$,$N^{\alpha}$-bis(carboxymethyl)-lysine (22 mg), 2-[methoxy(polyethylenoxy)$_{6-9}$propyl]-trimethoxysilane (22 mg), and 120 $\mu$L of 28% $NH_4OH$ solution. After 12 h stirring, the $SiO_2$-TMR-NTA was collected by centrifuging at 2000 rpm using 15 mL capacity 30K cutoff Amicon membrane filter and washing twice with ethanol adjusted to contain a final concentration of 5% ammonium hydroxide and finally with water. This solution was transferred to a conical 50 mL plastic tube. After standing overnight, precipitated material was eliminated by decanting and collecting the supernatant. The supernatant was stored in water used in further experiments. For spectral analysis, the $SiO_2$-TMR-NTA powder was obtained by lyophilization. See IR spectrum (Figure S3-1).

**Titration with $Ni^{2+}$ and Preparation of $SiO_2$-TMR-NTA-$Ni^{2+}$.** $NiCl_2 \cdot 6H_2O$ (2 mL, 0.1 M in deionized water) was added to $SiO_2$-TMR-NTA (11.1 mg) in deionized water, which was adjusted to ~pH 8 with 0.1 N NaOH (400 $\mu$L). The pale blue color still remained in solution. The particle was washed with water (2 mL × 3) by centrifuging at 2500 rpm. The collected washing solution and remaining particles were separately lyophilized to obtain an accurate weight to determine the change in mass. The dried particles (13.3 mg) were obtained as a reddish powder. Lyophilization of the washing solutions gave a residue that weighed 45.1 mg. The increased mass of $SiO_2$-TMR-NTA to form $SiO_2$-TMR-NTA-$Ni^{2+}$ ($2H_2O$, $Na^{+1}$) and the decreased mass of $NiCl_2 \cdot 6H_2O$ (corrected for inclusion of 2 equiv of NaCl that were liberated) matched exactly, being equivalent to $1.89 \times 10^{-5}$ mol/13.3 mg. See IR spectrum (Figure S4) and XPS data (Figure 1 and S6).

**Determination of the Number of Encapsulated TMR Fluorophore Molecules in a Silica Particle.** To determine the number of encapsulated TMR in a single particle, a 1 mM stock solution of 5(6)-carboxyTMR in ethanol was prepared. This solution was diluted into the same buffer to make four different solutions at final concentrations of 1.0 nM. The emission intensity of these solutions ($3.61 \times 10^{11}$ TMR molecules, 600 $\mu$L in 800 $\mu$L curvette) was measured and expressed as cps (count per second) using a fluorometer (excitation 545 nm and emission 575 nm) at 25 °C. The 1.25 mg (~$1.00 \times 10^{14}$ particles) of $SiO_2$-TMR was dispersed into 1 mL of ethanol, and this solution was diluted 100-fold twice. The emission intensity was measured after serially 2-fold diluting the stock solution until emission readings close to those of the 1.0 nM 5(6)-carboxy TMR solutions were obtained with less than 1% counting error range between the 1 nM TMR and sample $SiO_2$-TMR solution. The encapsulation number of the fluorophore was calculated by dividing the number of TMR matching reference 5(6)-carboxy TMR cps by number of particles.

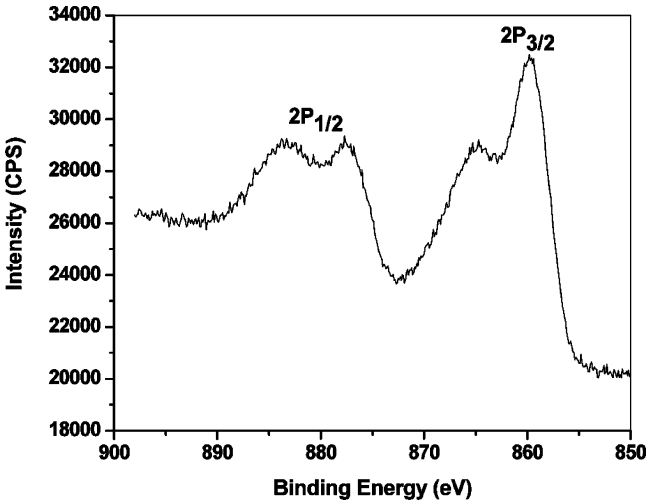


***Figure 1.*** X-ray photoelectron spectroscopic (XPS) data of $SiO_2$-TMR-NTA-$Ni^{2+}$ (**1**), showing the Ni ion peak section.

**Titration of $SiO_2$-TMR-NTA-$Ni^{2+}$ Particles (1) with a His-Tagged Peptide ((Fl)-MGHHHHHHS-COOH).** $SiO_2$-TMR-NTA-$Ni^{2+}$ particles (**1**, 86 $\mu$g) were suspended in pH 7.5 sodium bicarbonate buffer (200 $\mu$L), and 20 $\mu$L of (Fl)-NH-MGHHHHHHS-COOH (Fl-$His_6$) (1 mM in deionized water) was added to the suspension. After 5 min, the supernatant and particles were separated by centrifuging at 4000 rpm. The captured Fl-$His_6$ was detached by treating with buffer A (20 mM Tris-HCl, pH 8.0 containing 500 mM NaCl, 10% glycerol, and 10 mM $\beta$-mercaptoethanol) containing 500 mM imidazole. The fluorescein UV absorption intensity of the resulting solution and of the supernatant was measured at 496 nm in 0.1 N NaOH solution, using an appropriate volume so that the absorption measured was in the range of the standard curve. The standard correlation curve was prepared by measuring the absorption of 10, 5, 2.5, 1.25 mM of Fl-$His_6$ in 0.1 N NaOH aqueous solution. (Figure S5, left). Calculations based on the UV absorption intensity indicated that the recovery of Fl-$His_6$ from the supernatant was $12 \times 10^{-9}$ mol, and from the particle extract was $7.2 \times 10^{-9}$ mol, based on 86 $\mu$g of particles. Based on the amount of Fl-$His_6$ taken up by the particles, 96% was recovered from the beads.

**Association and Dissociation (Isolation and Purification) of ER$\alpha$ LBD with $SiO_2$-TMR-NTA-$Ni^{2+}$ Nanoparticles (1).** The cloning and bacterial expression of ER$\alpha$ LBD (304-554) as a $His_6$-fusion protein and its estradiol binding activity have been described previously.[17] The bacterial pellet from 250 mL of culture was lysed by sonication in buffer A (described above). The estradiol binding activity of the lysate was found to be 0.24 mg/mL. Nanoparticle **1** was suspended as 1 mg/mL solution in buffer B (20 mM Tris-HCl, pH 8.0 containing 150 mM NaCl, 10% glycerol, and 10 mM $\beta$-mercaptoethanol). To determine the $His_6$-protein capacity of particles **1**, 50 $\mu$L of the solution of **1**, containing 50 $\mu$g, was transferred to 1.0 mL microcentrifuge tubes and spun for 2500*g* for 5 min to remove the clarified buffer solution. Packed particles **1** were suspended and incubated for 20 min at room temperature with indicated amounts of bacterial lysate in a final volume

(17) Carlson, K. E.; Choi, I.; Gee, A.; Katzenellenbogen, B. S.; Katzenellenbogen, J. A. *Biochemistry* **1997**, *36*, 14897−905.

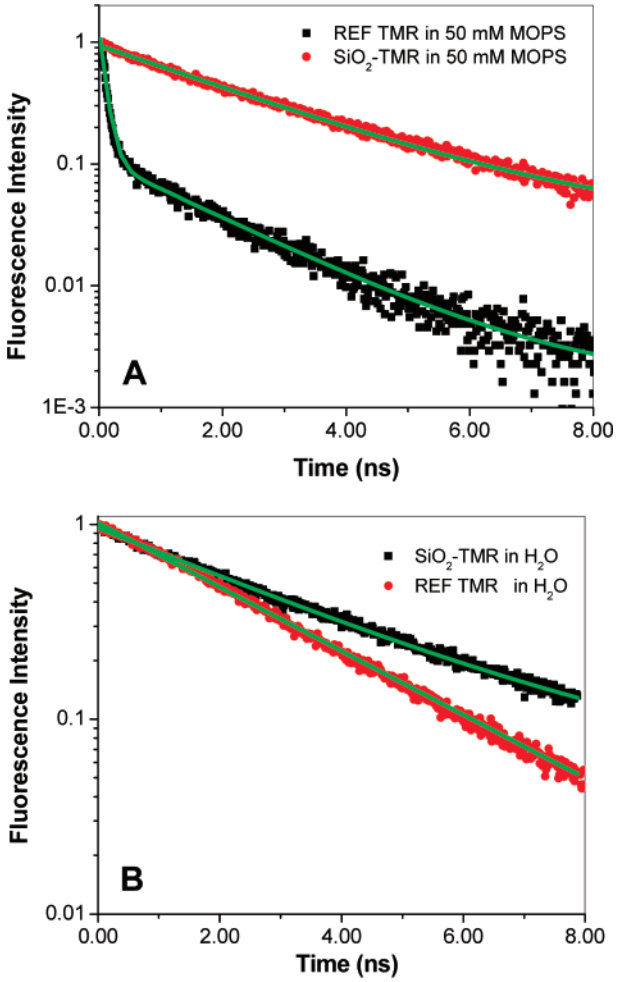


***Figure 2.*** Time-correlated single photon counting for TMR (free molecule) and the nanoparticle $SiO_2$-TMR in pH 8 MOPS buffer (panel A) and in deionized (DI) water (panel B) is plotted logarithmically against time on the nanosecond time scale at 25 °C at the magic angle. The decay curves obtained from $SiO_2$-TMR in DI water (B, black dots), in pH 8 MOPS buffer (A, red dots), and free reference 5-carboxy-TMR in DI water (B, red dots) were well fitted with a first-order exponential function ($y = A$*exp($-t/\tau$) + $y_0$). The decay of free reference 5-carboxy-TMR in pH 8 MOPS buffer (A, black dots) was fitted with a biexponential function ($y = A_1$*exp($-t/\tau_1$) + $A_2$*exp($-t/\tau_2$) + $y_0$).

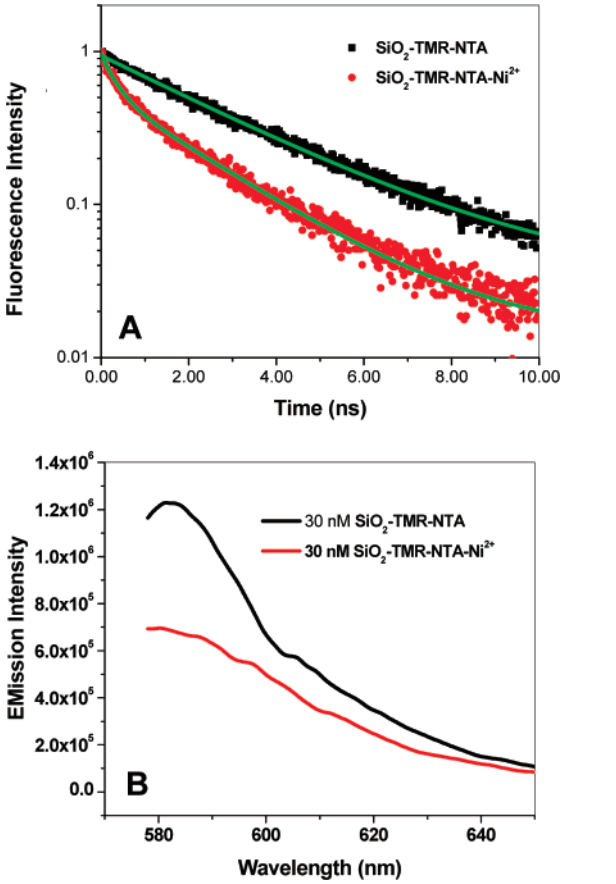


***Figure 3.*** Time-correlated single photon counting for the $SiO_2$-TMR-NTA and $SiO_2$-TMR-NTA-$Ni^{2+}$ particles (**1**) in DI water is plotted logarithmically against time on the nanosecond time scale at 25 °C at the magic angle (panel A). The decay curves obtained from $SiO_2$-TMR-NTA (black dots) and $SiO_2$-TMR-NTA-$Ni^{2+}$ (**1**, red dots) in DI water were well fitted to a single-exponential function ($y = A$*exp($-t/\tau$) + $y_0$) for $SiO_2$-TMR-NTA and a biexponential function ($y = A_1$*exp($-t/\tau_1$) + $A_2$*exp($-t/\tau_2$) + $y_0$) for $SiO_2$-TMR-NTA-$Ni^{2+}$. The green lines represent the line from the fitting functions. The quantitative quenching effect caused by the addition of $Ni^{2+}$ ($SiO_2$-TMR-NTA vs $SiO_2$-TMR-NTA-$Ni^{2+}$) was determined by fluorometry ($\lambda_{ex}$ 558 nm) (panel B).

of 75 $\mu$L; reaction volume was adjusted with buffer A. The nanoparticles were washed three times each with buffers A and B (500 $\mu$L) containing 5 mM imidazole by centrifugation at 2500*g*. Bound ERα LBD was dissociated with buffer A containing 500 mM imidazole, and the estradiol binding activities in the dissociated protein fraction and the nanoparticles after imidazole dissociation were determined by a radiometric binding assay (Figure 5B), as described previously.[17] Purity of the dissociated protein was assessed by electrophoresis in an 8% SDS-polyacrylamide gel (Figure 5A).

**MALDI-TOF Mass Analysis of ERα Anchored on the NTA-$Ni^{2+}$-Modified Silica Particles and Unmodified Silica Particles.** Interestingly, direct MALDI-TOF MS analysis of the proteins anchored on the $SiO_2$-TMR-NTA-$Ni^{2+}$ nanoparticles (**1**) after exposure to the lysate and washing with the 5 mM imidazole-containing buffers gave a very high-intensity signal only for ERα-LBD (Figure S6). Significantly, similar MALDI-TOF MS analysis of $SiO_2$-TMR NPs (i.e., those lacking the NTA-$Ni^{2+}$ tether for the His X 6 tag) after exposure to the same bacterial lysate failed to show any signals for ERα-LBD (Figure S6), indicating that the association of ERα-LBD was dependent on the NTA-$Ni^{2+}$ group and that nonspecific adsorption is minimal.

**Fluorescence Lifetime Measurements.** Time-correlated single photon counting was performed using a femtosecond Ti:sapphire laser (Tsunami, SpectraPhysics) whose fwhm (full width at half-maximum) pulse was measured to be 100 fs. The repetition rate was 80 MHz, and the wavelength was 800 nm. The experiments were carried out within a homemade microscope. An Avanlanche Photodiode detector (id100-20, id Quantique) was used to detect the fluorescence. The signal was input to the time-to-amplitude converter as a start signal followed by a constant fractional discriminator (Becker & Hickel GmbH, TC-SPC730). In this setup, the total instrument response function was around 40 ps at fwhm (full width at half-maximum). The data obtained from this instrument were analyzed with Origin 7.5 software.

**Protein Expression.** The ligand binding domain (LBD) of the human estrogen receptor alpha (ERα, amino acids 304−554) was expressed in *E. coli*, using methods reported previously.[17] For the microarray experiments, a mutant ERα LBD, with a single reactive cysteine at 417, was labeled in a site-specific manner with one fluorophore per protein, as previously reported.[18] The steroid receptor coactivator nuclear receptor domain (SRC-3-NRD, amino acids 627−829) was expressed, purified, and fluorescein labeled using methods reported previously.[19]

**Dynamic Light Scattering Measurement.** Data were collected with a DynaPro-MS/X instrument from Protein Solutions and evaluated with

(18) Tamrazi, A.; Katzenellenbogen, J. A. *Methods Enzymol.* **2003**, *364*, 37−53.
(19) Tamrazi, A.; Carlson, K. E.; Rodriguez, A. L.; Katzenellenbogen, J. A. *Mol. Endocrinol.* **2005**, *19*, 1516−28.

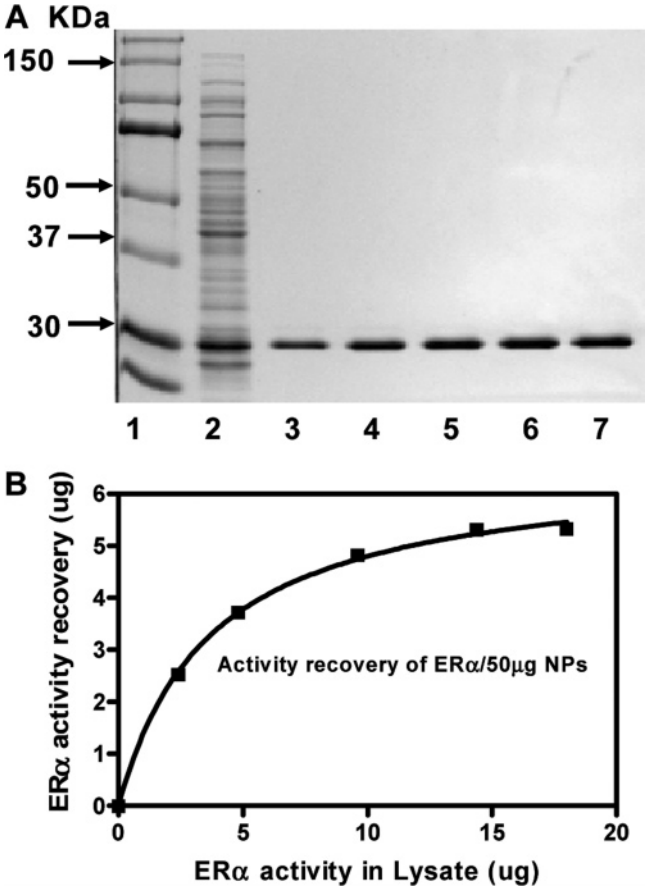


***Figure 4.*** Gel electrophorogram of purified ERα protein (lane 1, marker; lane 2, lysate; lanes 3−7, 2.4, 4.8, 9.6, 14.4, 18 $\mu$g of amounts of lysate loaded onto 50 $\mu$g of $SiO_2$-TMR-NTA-$Ni^{2+}$ particles **1**) (panel A) and their binding capacity (panel B), determined radiometrically.[17]

the DYNAMICS V6 software. $SiO_2$-TMR and **1** were measured in the 20% ethanolic aqueous solution at a 90° scattering angle at 25 °C. The ERα protein and $SiO_2$-TMR-NTA-$Ni^{2+}$-ERα were measured in Tris buffer (50 mM Tris containing 10% glycerol). The ERα protein was passed through a 0.2 $\mu$m membrane filter before measuring. Whole samples were adjusted to 0.05 mg/mL for measurement. For each sample, 20−25 data points were collected. Mean values were calculated for the DLS parameters. The autocorrelation function of intensity was analyzed by the cumulants analysis method to obtain the average diffusion coefficient, $D$, of the particles and the polydispersity. The hydrodynamic diameter, $D_h$, was calculated from the Stokes−Einstein equation ($D_h = \kappa_B T/3\pi\eta D$, where $\kappa_B T$ is the thermal energy and $\eta$ is the viscosity of the continuous phase). The resulting diagram (Figure S5) was created by Origin 7.5 graphics software.

**Particle Density.** The density of $SiO_2$-TMR-NTA-$Ni^{2+}$ (**1**) and $SiO_2$-TMR was determined as follows: Dried NPs were added to a volumetric flask (2 mL) filled with deionized water at 25 °C. The NPs were completely dispersed in the solution. The NPs were spin down by centrifugation at 4500 rpm. The increased volume was determined and used to calculate the density. The densities of $SiO_2$-TMR and $SiO_2$-TMR-NTA-$Ni^{2+}$ were determined to be 1.98 and 2.13, respectively.

**FRET Assay with the 1:76 Ratio of $SiO_2$-TMR-NTA-$Ni^{2+}$-ERα to Cy5-SRC1 Box II Peptide (Cy5-LTERHKILHRLLQEGSPSD-COOH) in Buffer Solution.** The particles stock solution was prepared by diluting $SiO_2$-TMR-NTA-$Ni^{2+}$-ERα (1, $14.4 \times 10^{11}$ particles, 18 $\mu$L taken from 1 $\mu$g/100 $\mu$L in pH 8.0, 50 mM MOPS buffer containing 10% glycerol) with 1782 $\mu$L in the same buffer. The 1800 $\mu$L stock solution was divided into three 600 $\mu$L portions in 1 mL plastic conical tubes. Each solution contains $4.8 \times 10^{11}$ particles. To each tube was added Cy5-SRC1 NR box II peptide ($3.6 \times 10^{13}$ molecules, 0.6 $\mu$L taken from 100 $\mu$M stock solution) in the same buffer solution. Subsequently, 0.6 $\mu$L of 100 $\mu$M estradiol ($E_2$) and TOT in the same buffer was added to each premixed solution. To the remaining tube was added 0.6 $\mu$L of the same buffer solution as in an APO measurement. After 30 min incubation at room temperature with protection from light, emission intensity (578−700 nm) was measured in an 800 $\mu$L quartz cuvette with a fluorometer with excitation at 558 nm. (This experiment was also carried out under the same condition as above, except at a 1:29 ratio of $SiO_2$-TMR-NTA-$Ni^{2+}$-ERα to Cy5-SRC1 box II peptide. In this case, to Cy5-SRC1 box II peptide ($1.4 \times 10^{13}$ molecules, 0.24 $\mu$L taken from 100 $\mu$M stock solution) was added 600 $\mu$L of $SiO_2$-TMR-NTA-$Ni^{2+}$-ERα ($14.4 \times 10^{11}$, 18 $\mu$L taken from 1 $\mu$g/100 $\mu$L in pH 8.0, 50 mM MOPS buffer containing 10% glycerol), and the experiment was conducted as above.) To observe a detachment of ERα from $SiO_2$-TMR-NTA-$Ni^{2+}$, imidazole (0.6 $\mu$L, 0.1 M in water) was added to 600 $\mu$L of premixed $SiO_2$-TMR-NTA-$Ni^{2+}$-ERα and Cy5-SRC1 box II peptide solution after measurement in the presence of $E_2$ (1 $\mu$M).

**Microarray Assays. (A) Printing SRC3-Fl and SRC3 on an Aldehyde Slide and Recruitment of $SiO_2$-TMR-NTA-$Ni^{2+}$-ERα.** A 0.1-$\mu$L volume of 3 $\mu$M SRC3-Fl and SRC3 in 50 mM MOPS, pH 8.0, 40% glycerol buffer was spotted on the aldehyde glass slide (Telechem, Sunnyvale, CA) in duplicate using a micropipette tip. After printing, the slides were allowed to incubate for 2.5 h, at 65−70% humidity and at 15 °C. Each subarray was isolated by a hydrophobic barrier drawn with a pap pen. The slide was then washed and blocked in 3% BSA in 50 mM MOPS buffer, pH 8.0, 0.01% sodium azide. The first wash was done by dipping the slide directly face down into the BSA-MOPS buffer. It was then incubated in ~50 mL of BSA-MOPS buffer at room temperature, with gentle agitation for 1 h.

**(B) $SiO_2$-TMR-NTA-$Ni^{2+}$-ERα** (20 nM) with either estradiol (100 nM), ICI164,384 (100 nM), or without ligand in 3% BSA-MOPS buffer was added to the box defined by the pap pen lines, and this was incubated at room temperature for 1 h in the dark. The unbound ligand was removed by a brief wash in the same buffer. The slide was dried by centrifugation for 1 min at 1500 rpm (400*g*) in a disposable 50 mL centrifuge tube with an absorbent pad in the bottom.

**(C) Imaging.** Imaging was done on a GenePix 4000 dual-laser scanner at 535 and 635 nm (Axon Instrument, Inc, Union City, CA) to produce an emission image at 575 nm (BP 25 nm). The laser was powered by GenePix Pro 4.0. The PMT voltage was set between 500 and 600, and the gain was set to 33%. A Typhoon 9400 multilaser scanner (Amersham Biosciences, Sunnyvale, CA) was used to obtain 490 nm excitation and 590 nm emission (bandpass 15 nm) with 650 PMT, and the image of emission intensity was rendered in false color, from red for high to green for low.

## 3. Results and Discussion

**3.1. Synthesis and Physical, Spectroscopic, and Photophysical Characterization of TMR-Doped Nickel NTA-Modified Silica Nanoparticles ($SiO_2$-TMR-NTA-$Ni^{2+}$, 1). Synthesis of Various TMR-Doped Silica Nanoparticles: Size and Spectroscopic Characterization.** The TMR-doped silica nanoparticles were synthesized by the method of Stöber,[20] with modifications to covalently conjugate 5-carboxy-TMR to the silica particles, as described in the literature.[7] Scheme 1 illustrates a representative preparation of TMR-doped silica particles, their use in a purification of a histidine-tagged protein, and their direct application to a protein−protein interaction assay in a microarray system or in solution phase.

The underivatized $SiO_2$-TMR, prepared in ethanol, had a narrow size distribution (~23 nm, as determined by transmission electron microscopy (TEM), ~25 nm as determined by DLS;

(20) Stöber, W.; Fink, A.; Bohn, E. *J. Colloid Interface Sci.* **1968**, *26*, 62−9.

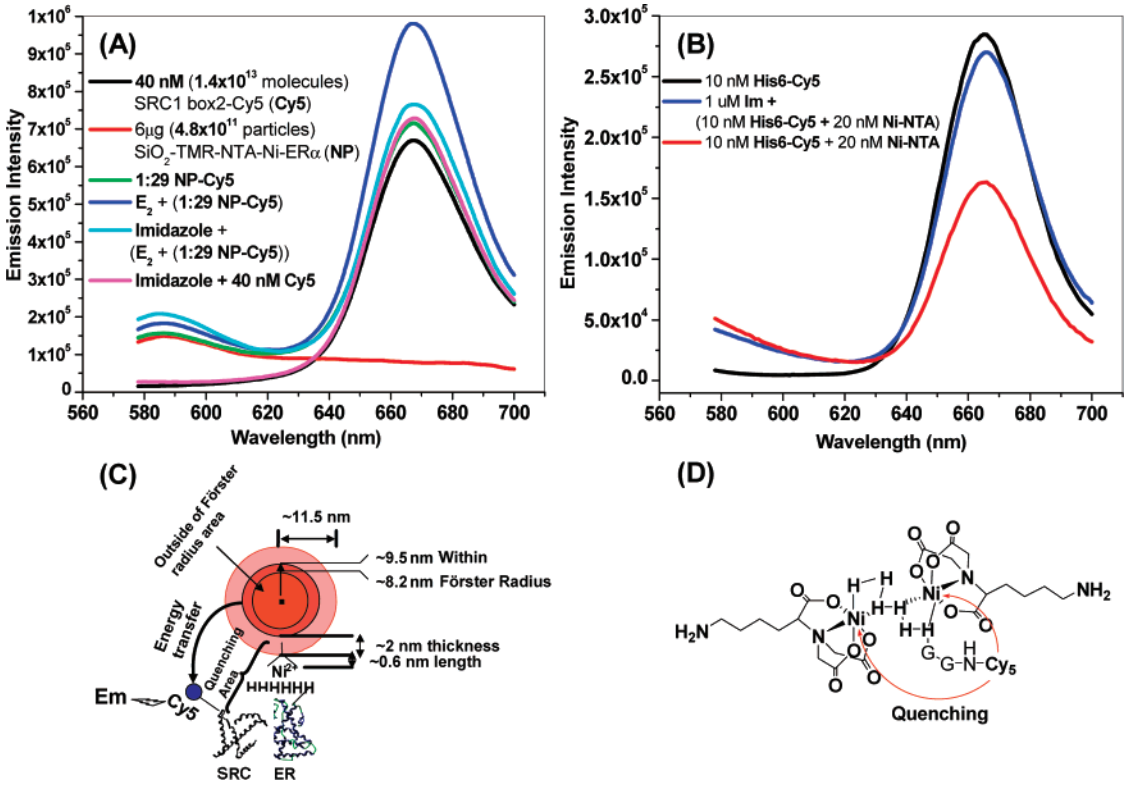


***Figure 5.*** Interaction between $SiO_2$-TMR-NTA-$Ni^{2+}$-ERα and SRC1 box2-Cy5 (SRC-Cy5) at the ratio of 1:29 under various conditions ($\lambda_{ex}$ 558 nm) (A) and nickel quenching effect by adding 2 equiv of Ni-NTA system to $His_6$-Cy5 (HHHHHHGG-Cy5) (ex 558 nm) (B). Schematic illustration of geometric factors in $SiO_2$-TMR-NTA-$Ni^{2+}$ with particle-anchored ERα and SRC-Cy5 (C) and Ni-NTA and $His_6$-Cy5 interaction (D).

see Supporting Information Figures S3-2 and 5). FTIR characterization of this material (see Supporting Information Figure S1) showed bands at 459.2, 797.5, and 1081 $cm^{-1}$ from Si−O−Si bending, cage motion, and Si−O−Si stretching modes, respectively. XPS showed peaks corresponding to Si2p, O1s, and N1s bands (see Supporting Information Figure S7).

To prepare the nickel NTA-modified TMR-doped silica nanoparticles ($SiO_2$-TMR-NTA-$Ni^{2+}$, **1**), the silane-substituted NTA conjugate **5**, obtained by reaction of the silane isocyanate **2** with the protected NTA precursor **3** followed by acid deprotection of the *t*-butyl esters, was subjected to controlled hydrolysis together with the TMR-doped silica nanoparticles ($SiO_2$-TMR) and a polyethyleneglycol silane [$(MeO)_3Si$-$(CH_2)_3$-$(OCH_2CH_2)_{6-9}OMe$]. Final exposure to $NiCl_2$ gave the fully functionalized TMR-doped and Ni-NTA-modified nanoparticles, $SiO_2$-TMR-NTA-$Ni^{2+}$ (**1**), which we found were readily dispersible in water and formed a stable suspension that did not settle.

The $SiO_2$-TMR-NTA-$Ni^{2+}$ particles (**1**) were characterized by FTIR and XPS. The TEM image again revealed very narrow size distribution (~23 nm, also ~28 nm by DLS; see Supporting Information Figure S5). The Si−O−Si bending, silicon cage motion, and Si−O−Si stretching frequencies of both $SiO_2$-TMR-NTA (without nickel) and $SiO_2$-TMR-NTA-$Ni^{2+}$ (with nickel) appeared at wavelengths similar to that of unmodified $SiO_2$-TMR. The tricarboxylate stretching frequency in the NTA system appeared as a strong band at 1614 $cm^{-1}$, which shifted to 1599 $cm^{-1}$ in the NTA-$Ni^{2+}$ chelate (see Supporting Information, Figure S3-1). X-ray photoelectron spectroscopy (XPS) of **1** shows a peak at 859 eV corresponding to Ni ($2p_{3/2}$), as shown in Figure 1.

**Photophysical Characterization of the TMR-Doped Silica Nanoparticles: Lifetime, Quantum Yield, and Nickel Quenching Effect.** To investigate the stability and relative quantum yield of the TMR-doped silica particles ($SiO_2$-TMR), as compared to free 5-carboxy TMR as a reference, fluorescence lifetime measurements were made with $SiO_2$-TMR and 5-carboxy-TMR using a time-correlated single photon counting system. Plots of the fluorescence intensity with time are shown in Figure 2, and the lifetime data are summarized in Table 1. Because the scattering properties of the silica nanoparticles made absorbance determinations difficult, we used lifetime measurements to estimate their relative quantum yields using the simple equation below,[21] rather than conventional quantitative absorbance and emission measurements.

$$Q = \tau/\tau_n$$

where $\tau$ is the measured lifetime, $\tau_n$ is the natural lifetime of the reference dye, and $Q$ is the quantum yield.

While 5-carboxy TMR has a lifetime of 2.7 ns in deionized (DI) water, which is ~10% greater than that reported for TMR in tris buffer,[22] it is substantially quenched in pH 8 MOPS buffer, with a major component (91%) having a 0.1 ns lifetime and a minor component (9%) retaining the longer lifetime. By contrast, TMR embedded in $SiO_2$ ($SiO_2$-TMR), regardless of whether it is in DI water or MOPS buffer, shows a single-exponential decay (ca. 2.5−3.0 ns) comparable to that of TMR in DI water. This means that the TMR molecules that are encapsulated inside the $SiO_2$ particles are shielded from

(21) Lakowicz, J. R. *Principles of Fluorescence Spectroscopy*, 2nd ed.; Kluwer Academic/Plenum Publishers: New York, 1999; pp 10−11.
(22) Edel, J. B.; Eid, J. S.; Meller, A. *J. Phys. Chem. B* **2007**, *111*, 2986−2990.

***Scheme 1.*** Schematic Illustration of the Preparation for NTA-Modified Dye-Embedded Silica Nanoscale Particles for Site-Specific Immobilization of a Histidine-Tagged Protein (Estrogen Receptor, ER) and Direct Application to ER-SRC Interaction Fret Assay in Solution or on a Microarray[a]

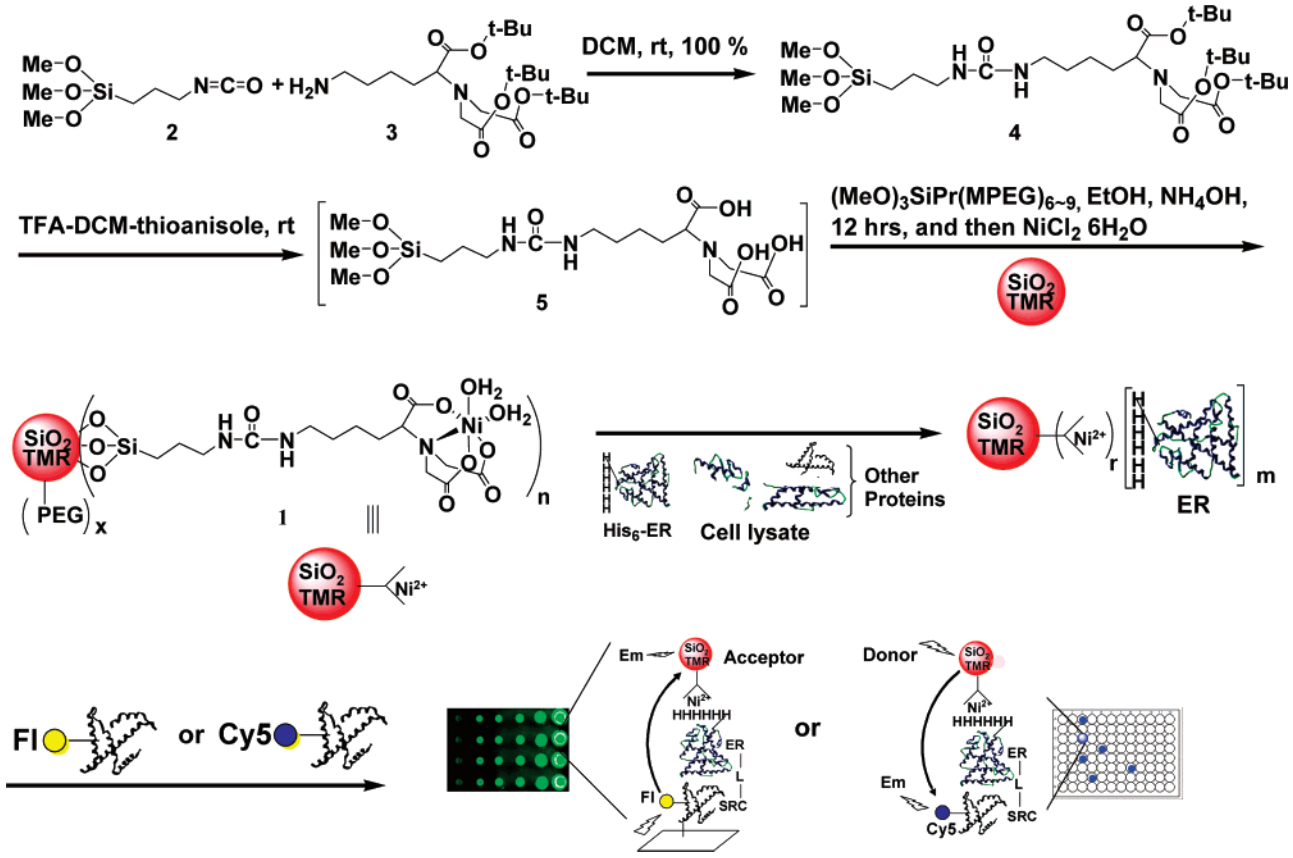


[a] The small characters after the parentheses (*x*, *n*, and *m*) indicate multiple attachments.

***Table 1.*** Fluorescence Lifetime Data for Reference 5-Carboxy-TMR and $SiO_2$-TMR in Deionized (DI) Water and pH 8 MOPS Buffer and $SiO_2$-TMR-NTA and $SiO_2$-TMR-NTA-$Ni^{2+}$ in DI Water

| | reference 5-carboxy TMR | | $SiO_2$-TMR | | $SiO_2$-TMR-NTA | $SiO_2$-TMR-NTA-$Ni^{2+}$ |
|---|---|---|---|---|---|---|
| | DI water | pH 8 MOPS buffer | DI water | pH 8 MOPS buffer | DI water | DI water |
| $\tau_1$[a] (population)[b] | 2.73 | 0.10 (91%) | 3.20 | 2.40 | 3.00 | 0.35 (44%) |
| $\tau_2$[a] (population)[b] | | 1.78 (9%) | | | | 2.32 (56%) |
| excitation (nm) | 553 | 553 | 558 | 558 | 558 | 558 |
| emission (nm) | 578 | 578 | 583 | 583 | 583 | 583 |

[a] Lifetimes are given in nanoseconds. [b] The number in parentheses denotes relative percent ampliduce obtained from the biexponential fit (see Figure 2 legend).

the quenching species in the MOPS buffer and are able to retain their native radiative properties. Thus, silica-embedded TMR is a more robust fluorophore than TMR in aqueous solution, a favorable characteristic for quantitative fluorometric assays.

The lifetime of $SiO_2$-TMR is actually 17% longer than that of TMR. Because quantum yield is proportional to fluorescence intensity, which is proportional to lifetime,[21] we can estimate that the quantum yield of TMR in the $SiO_2$-TMR particles is ~17% greater than that of free TMR in DI water. Thus, on the basis of literature values for the quantum yield of TMR (~0.81 in water),[23] we expect the quantum yield of TMR in the $SiO_2$-TMR particles to be ~0.95. The excitation and emission of free TMR and TMR $SiO_2$-TMR are only slightly shifted, from 553 to 557 nm for excitation and from 578 to 583 nm for emission.

In related work, Santra[24] reported that free fluorescein showed a single exponential, but also found that fluorescein encapsulated in a $SiO_2$ matrix showed a double exponential function, with a longer lifetime than free fluorescein in EtOH water. Wisner's group[8] also reported a longer lifetime for tetramethyl rhodamine isothiocyanate when encapsulated in a $SiO_2$ matrix. The good stability and single-exponential decay of $SiO_2$-TMR in pH 8 buffer is beneficial in its applications in fluorometric and FRET experiments involving proteins.

As is explained in the Experimental Section, we can estimate the number of silica nanoparticles in solution, and, by fluorometric comparison of the TMR-doped $SiO_2$ particles with free TMR, we estimate that on the average there are the equivalent of 860 TMRs encapsulated in each $SiO_2$-TMR particle. Considering the somewhat greater quantum yield for TMR in the

(23) Olmsted, J., III. *J. Phys. Chem.* **1979**, *83*, 2581−4.

(24) Santra, S.; Liesenfeld, B.; Bertolino, C.; Dutta, D.; Cao, Z.; Tan, W.; Moudgil, B. M.; Mericle, R. A. *J. Lumin.* **2006**, *117*, 75−82.

particle, as determined from the lifetime measurements conducted above, we estimate that there are, in fact, somewhat fewer TMR molecules per particle, ca. 720.

After modification of the surface of the $SiO_2$-TMR particles with the NTA function, the fluorescence decay of $SiO_2$-TMR-NTA was found to be a single exponential with a lifetime of 3.0 ns (see Figure 3A, black dotted line); this is only ~7% shorter than that of the unmodified $SiO_2$-TMR particles, but still ~10% longer than free TMR (~2.7 ns, see Table 1). Addition of nickel to form $SiO_2$-TMR-NTA-$Ni^{2+}$ particles (**1**), however, shifted the decay to a biexponential (Figure 3A, red dotted line, Table 1), with about one-half of the species retaining the longer lifetime. We interpret this to be the result of quenching by the surface-bound $Ni^{2+}$ ion that affects ca. 44% species of the TMR in the $SiO_2$ particles, presumably those that are close to the particle surface, reducing their lifetime to 0.35 ns. The remaining 56% of the TMR molecules, however, presumably those more deeply embedded in the particles, are less affected by this quenching phenomenon, retain a characteristic long lifetime (2.3 ns), and can efficiently participate in the fluorometric and energy transfer for assays. We do not know for certain whether the 23% reduction in the lifetime of the long-lived species (from 3.0 to 2.3 ns) is caused by nickel quenching. Nevertheless, on the basis of these results, we can make an estimate of how many TMR molecules are within the Förster radius between TMR and Cy5 used in the FRET experiments but are also not quenched by nickel, so that they are able to participate efficiently in energy transfer (see below).

We have also directly determined the reduction of TMR emission intensity by comparing the fluorescence of the $SiO_2$-TMR-NTA particles in the absence and presence of $Ni^{2+}$ ion, as shown in Figure 3B. These spectra show that the TMR emission intensity is reduced ~43% in the presence of $Ni^{2+}$ ion, a reduction very close to that obtained from the lifetime measurements (Figure 3A). Conventional fluorometry, however, does not allow one to characterize the two distinct TMR lifetimes that are observed in the lifetime measurements (Figure 3A).

If we hypothesize that TMR is evenly distributed throughout each silica particle, we can calculate the fraction of TMR molecules in shells of different thicknesses at various distances from the particle surface. With a particle having a diameter of ~23 nm (radius of 11.5 nm) based on the TEM image, ~44% of the total TMRs in the particle would be within ~2 nm range from surface. (This 2 nm shell represents 44% of the total volume of a 23 nm particle.) Because this represents the percent of TMR that appears to be quenched by the nickel, we take this to be a reasonable estimate of the depth to which the nickel quenching effect is operating, although this quenching is obviously a progressive, distance-dependent phenomenon. If we assume that the nickel atoms are ~0.6 nm from the particle surface (based on an estimate of the length of the NTA silane structure, obtained using molecular modeling using SYBYL software), then we can approximate the range of efficient quenching by the Ni ions to be ~2.6 nm (the sum of the 2 nm depth of the efficient quenching effect plus the 0.6 nm nickel-to-particle surface distance).

The reported Förster radius between TMR and Cy5 is between 6.5 and 7.1 nm.[25−27] Taking 6.5 nm as the Förster radius, the total number of TMR molecules within Förster radius can be estimated by calculating the volume of a shell in a 23 nm diameter particle (by TEM) between radii of 8.2 and 9.5 nm, determining this as a fraction of the total particle volume, and multiplying this by 720 (the number of TMR molecules estimated to be in the particle, see above). The 8.2−9.5 nm radius shell represents the portion of the particle that is beyond the effective nickel quenching distance yet within the Förster radius for the TMR-Cy5 combination. The volume of this shell is ~20% the volume of the particle, and ~20% of the TMRs estimated to be in each particle is ~140, which we believe is the number of TMRs that are within the Förster distance for a TMR-Cy5 pair and thus able to function efficiently as donors to Cy5 in a FRET experiment between the TMR-doped $SiO_2$-TMR-NTA-$Ni^{2+}$ particles (**1**) and a Cy5-labeled protein.

**3.2. Binding Capacity of $SiO_2$-TMR-NTA-$Ni^{2+}$ Particles (1) and Purification of the Estrogen Receptor (ERα). Estimation of Surface Functionalization Density and His-Tagged Peptide and Protein Binding Capacity.** Also relevant to the quantitative aspects of various fluorometric or FRET experiments using the $SiO_2$-TMR-NTA-$Ni^{2+}$ particles (**1**) is the number of NTA-$Ni^{2+}$ functionalities present on the particle surface and the degree to which steric factors might constrain the binding of his-tagged peptides and proteins (such as the estrogen receptor α ligand binding domain, ERα). We have estimated these capacity values by titration with fluorescein-labeled 6x histidine peptide and ERα.

The capacity by titration with fluorescein-labeled oligohistidine-containing peptide (Fl)-NH-MGHHHHHHS-COOH (designated as Fl-$His_6$) is 84 nmol/mg, which would correspond to 670 Fl-$His_6$ bound per particle (see Experimental Section). The capacity and specificity for anchoring a His-tagged protein to a $SiO_2$-TMR-NTA-$Ni^{2+}$ particle (**1**) was determined by adding different amounts of a cell lysate from *E. coli* containing bacterially expressed ERα ligand binding domain (designated simply as ERα) to particles **1** dispersed in buffer solution. Protein loading capacity, evaluated radiometrically by ligand binding after protein elution,[17] saturated at 107 μg/mg, which corresponds to 3 nmol/mg of **1** or ~28 ERα proteins per particle, as shown in Figure 5. Presumably, reduced capacity of the particles for binding the protein is the result of the steric hindrance experienced by the larger protein as compared to the smaller peptide probe. The number for the protein, however, is very close to 33, the maximum number of ERα proteins per particle estimated from the size (area) of the ERα ligand binding domain, based on from X-ray crystal structures, and the calculated surface area of a nanoparticle (**1**).

The specificity of the interaction of ERα and the nanoparticles **1** is very high, as evident from the cleanness of the electrophorogram even at the highest loading (Figure 4A, lane 7). The high specificity was confirmed by MALDI-TOF mass spectrometry. Direct loading of $SiO_2$-TMR-NTA-$Ni^{2+}$-ERα onto the

(25) Deniz, A. A.; Dahan, M.; Grunwell, J. R.; Ha, T.; Faulhaber, A. E.; Chemla, D. S.; Weiss, S.; Schultz, P. G. *Proc. Natl. Acad. Sci. U.S.A.* **1999**, *96*, 3670−5.
(26) Sabanayagam, C. R.; Eid, J. S.; Meller, A. *J. Chem. Phys.* **2005**, *122*, 061103/1−061103/5.
(27) Ying, L.; Green, J. J.; Li, H.; Klenerman, D.; Balasubramanian, S. *Proc. Natl. Acad. Sci. U.S.A.* **2003**, *100*, 14629−34.

sample plate with matrix gave only a ~33 kDa ERα peak in the MADI-TOF spectrum (see Supporting Information Figure S6).

By DLS, we can indirectly verify that $SiO_2$-TMR-NTA-$Ni^{2+}$ forms a complex cluster with the ERα: The hydrodynamic diameter of the $SiO_2$-TMR-NTA-$Ni^{2+}$ particle (**1**) increases from 28 nm before the addition of ERα to 51 nm after the addition of ERα, as in $SiO_2$-TMR-NTA-$Ni^{2+}$-ERα (see Supporting Information Figure S5); the 23 nm increase in diameter is very close to twice the diameter of ERα (2 × ~9.8 nm = 19.6 nm), as would be expected if the $SiO_2$-TMR-NTA-$Ni^{2+}$ particles were fully covered with ERα.

On the basis of our estimates of the number of ERα molecules that are anchored on the surface of a particle (ca. 28) and the number of TMR molecules thought to be within Förster radius (both the long-lifetime species beyond the effective quenching distance of nickel, ca. 140, and the short-lifetime species within quenching area, ca. 310), we estimate that there are approximately 5 TMR molecules having long lifetime and 11 TMR molecules having short lifetime per Cy5 fluorophore in the anchored protein that can efficiently participate in energy transfer. In addition, there are ca. 260 TMR molecules beyond the Förster radius that would participate less efficiently in energy-transfer processes. Thus, the $SiO_2$-TMR-NTA-$Ni^{2+}$ dual-mode nanoparticles (**1**) provide multiple TMR molecules that have stable, long fluorescence lifetimes in a rigid environment that are available for participation in fluorometric assays and in energy-transfer processes in FRET assays.

**3.3. Application of $SiO_2$-TMR-NTA-$Ni^{2+}$ Particles (1) to Protein−Protein Interaction Assays in Solution and on Glass Microarrays. $SiO_2$-TMR-NTA-$Ni^{2+}$-ERα Cy5-SRC FRET Experiments in Solution: Specificity of Interaction and Limits of Nickel Quenching of Fluorophore Emission.** In this Article, we have focused on TMR-doped $SiO_2$ particles, because, as described above, TMR has good photostability and high quantum yield. In addition, TMR is well matched as an acceptor in a fluorescein-TMR FRET pair and as a donor in a TMR-Cy5 FRET pair.

In the photophysical experiments with the $SiO_2$-TMR-NTA-$Ni^{2+}$ particles (**1**), described above, we found that $Ni^{2+}$ quenched TMR fluorophores embedded in the silica particles to a depth that was within 2.6 nm from the nickel ions. We wanted to evaluate whether the TMR molecules in these particles that were beyond the range of nickel quenching yet within the Förster radius for a TMR-Cy5 pair were effective in resonance energy-transfer processes. For this purpose, we designed two systems (Figure 6C and D), as shown schematically at the bottom of Figure 5.

We first (Figure 5C) investigated the interaction between particles that were fully saturated with ERα ($SiO_2$-TMR-NTA-$Ni^{2+}$-ERα) and a Cy5-labeled peptide having a sequence corresponding to the second nuclear receptor interaction box of the steroid receptor coactivator, SRC1, Cy5-SRC (Cy5-NH-LTERHKILHRLLQEGSPSD-COOH) at a particle-to-SRC ratio of 1:29 (estimated to give an ER:SRC ratio of 1:1); the experiment was done in the presence of $E_2$, an estrogen agonist required to promote the ER-SRC interaction and with and without imidazole to interrupt the ER-NTA-Ni interaction.

When excited at the absorbance maximum for TMR (558 nm), $SiO_2$-TMR-NTA-$Ni^{2+}$-ERα by itself shows essentially no

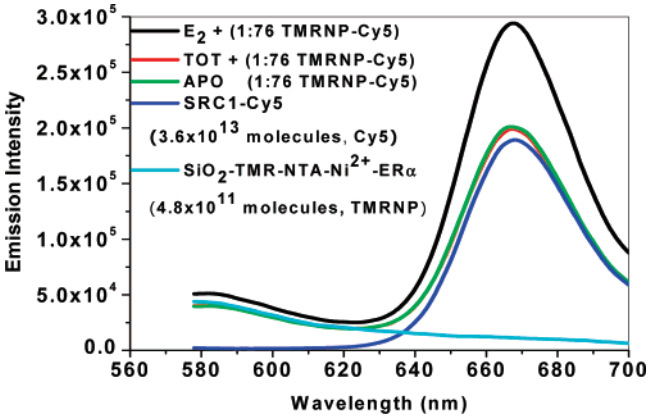


***Figure 6.*** FRET assay of $SiO_2$-TMR-NTA-$Ni^{2+}$-ERα with Cy5-SRC1 NR box II (Cy5-NH-LTERHKILHRLLQEGSPSD-COOH) in the presence of E2 (100 nM, agonist, black line), TOT (100 nM, antagonist, red line), and in the absence of ligand (APO, green line). Cy5-SRC1 NR box II (100 nM, dark blue line) and $SiO_2$-TMR-PEG-NTA-$Ni^{2+}$-ERα (light blue line) ($\lambda_{ex}$ 558 nm).

fluorescence at the wavelength of Cy5 emission (Figure 5A, 670 nm, red curve). A solution of Cy5-SRC gives an emission at 670 nm (black curve) that is unaffected by the addition of imidazole (purple curve) or of $SiO_2$-TMR-NTA-$Ni^{2+}$-ERα (without the agonist $E_2$; green curve). When $E_2$, which promotes the interaction of ER and SRC, is added to the mixture of Cy5-SRC and $SiO_2$-TMR-NTA-$Ni^{2+}$-ERα, the result is a 30% enhancement in emission due to FRET from the TMRs in $SiO_2$-TMR-NTA-$Ni^{2+}$-ERα to the Cy5 on the Cy5-SRC peptide (dark blue curve). The specificity of this interaction is indicated by the fact that addition of imidazole, which disrupts the interaction of ERα with the $SiO_2$-TMR-NTA-$Ni^{2+}$ particles (**1**), eliminates all of the enhanced Cy5 emission due to FRET (light blue curve). Thus, the $SiO_2$-TMR-NTA-$Ni^{2+}$ particles (**1**) are capable of engaging in FRET with Cy5-SRC through particle-bound ERα in the presence of an agonist ligand, $E_2$, which promotes ER-SRC interaction.

In this experiment, Cy5 does not appear to be appreciably quenched by nickel ion (see Figure 6A and C). Cy5 may be less prone to $Ni^{+2}$ quenching than TMR (see below), or it may simply be beyond the nickel quenching distance of 2.6 nm that we determined for TMR (see above). On the basis of molecular modeling, we estimate that the Cy5 is 1.1 nm from the **LHRLL** motif in the SRC1 box II peptide sequence (Cy5-LTERHKIL-HRLLQEGSPSD-COOH) and that the SRC binding groove in ERα is ~1.5 nm from the histidine tag to which the Ni-NTA is bound; the sum of these distances is 2.6 nm, the same as the range for Ni quenching of the TMR in the nanoparticle **1**. There also appears to be little nonspecific interaction between the nanoparticles **1** and the Cy5-labeled peptide.

FRET can be followed by increased acceptor intensity, decreased donor intensity, or both. Comparison of the light blue line (FRET) and the dark blue line (no FRET) shows that in this system the acceptor increase is very evident, but the donor decrease is minimal. We ascribe this to the fact that there are multiple donor TMRs in each nanoparticle, so FRET does not efficiently reduce donor emission intensity.

In the second experiment, we further investigated whether Cy5 might be quenched by nickel in a simple, small molecule Ni-NTA complex. As shown in Figure 5B and D, when Ni-NTA (40 nM; note, the small molecule, not the nanoparticle)

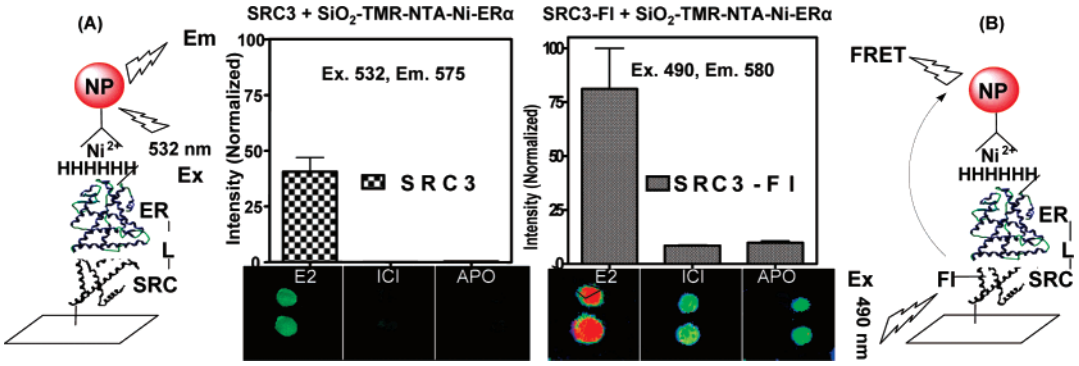


***Figure 7.*** Microarray false color image of SRC3-ERα interaction. Aldehyde slides were spotted with either SRC3-RID (i.e., with no fluorescein label, for the fluorometric assay, A) or with fluorescein-labeled SRC3-RID (for the FRET assay, B), and were then blocked with BSA. $SiO_2$-TMR-NTA-$Ni^{2+}$-ERα, liganded with agonist ($E_2$), antagonist (ICI), or no ligand (APO), was added. After washing, the slide for the fluorometric assay was scanned at ex 532 nm and em 575 ± 25 nm, and the quantification was plotted (A). Only TMR recruited by $E_2$ (agonist) in this fluorometric assay was detected. For the FRET assay, scanning was done at ex 490 nm and em 580 ± 15 nm, and the quantification was plotted (B). TMR FRET is shown as a false color image, generated using an option of pseudo false Color 1 of ImageQuant TL v2003.02: The red color corresponds to high emission intensity due to FRET between fluorescein on SRC3 and TMR encapsulated inside $SiO_2$-TMR-NTA-Ni-ERα; the green color corresponds to low a intensity emission from direct TMR excitation by the 490 nm excitation light (see text).

was added to a $His_6$-Cy5 peptide (20 nM) solution, the Cy5 emission was suppressed by 43%. Addition of imidazole (100 μM), which disrupts this interaction, restored 98% of the original Cy5 emission intensity. Thus, when Cy5 is close to the nickel center, its emission is appreciably quenched, but because quenching is a distant-dependent phenomenon, in most nanoparticle−protein interaction experiments using Cy5-labeled proteins, the Cy5 center will be sufficiently remote from the nickel centers of the $SiO_2$-TMR-NTA-$Ni^{2+}$ particles (**1**) so that this quenching should not interfere with fluorometric or FRET experiments (see Figure 5C). It is of note that when the same experiments were repeated using a $His_6$-TMR peptide, the extent of quenching by nickel was much greater (>75%, data not shown), indicating that the nickel quenching of Cy5 emission is considerably less than that of TMR emission.

**Use of $SiO_2$-TMR-NTA-$Ni^{2+}$ Nanoparticles (1) in Ligand-Dependent Estrogen Receptor-Coactivator Recruitment Experiments in Solution.** Having established the utility of the $SiO_2$-TMR-NTA-$Ni^{2+}$ nanoparticles (**1**) in FRET experiments, we further explored the specificity of ligand of different pharmacological classes in promoting the interaction between ERα on the $SiO_2$-TMR-NTA-$Ni^{2+}$ and Cy5 labeled SRC1-box2 (Cy5-SRC) in solution (Figure 6) or fluorophore-labeled SRC in a glass protein microarray system (Figure 7).[28,29] It is known that an agonist such as $E_2$ promotes the ERα-SRC interaction, whereas the interaction does not occur either in the absence of ligand (APO) or when ERα is bound to an antagonist.[28,29]

Usually when FRET assays are conducted with a low affinity protein as in this case (SRC1 box II peptide has $K_D$ of 1 μM), an excess of acceptor is used to ensure that the interaction is saturated. Nevertheless, as shown in Figure 5A, we observe a ~30% increase in acceptor intensity when $SiO_2$-TMR-NTA-$Ni^{2+}$-ERα and Cy5-SRC are in a 1:29 ratio, which corresponds to a 1:1 ratio in terms of ERα and Cy5-SRC. This demonstrates that our system has high sensitivity and should be useful in studying even relatively weak protein interactions. Although a 30% increase in acceptor emission is enough to observe this interaction, we typically increase the acceptor concentration to provide a 2−3-fold excess as compared to donor-labeled protein, because this gives a somewhat higher FRET signal.

The interaction of $SiO_2$-TMR-NTA-$Ni^{2+}$-ERα with Cy5-SRC ($\lambda_{ex}$ 558 nm, $\lambda_{em}$ 578−700 nm) showed a 53% increase in Cy5 emission in the presence of $E_2$ (agonist) as compared to those of TOT (antagonist) and APO (no ligand), consistent with FRET due to the $E_2$-mediated ER-SRC1 interaction (Figure 6). There is no ER-SRC interaction without ligand (APO) or with the antagonist (TOT), which is known to disable the agonist-mediated ER-SRC interaction. The Cy5 emission intensity in the APO and TOT experiments is just the same as the sum of the background emission of $SiO_2$-TMR-NTA-$Ni^{2+}$ and control Cy5.

The interaction of $SiO_2$-TMR-NTA-$Ni^{2+}$-ERα with Cy5-SRC ($\lambda_{ex}$ 558 nm, $\lambda_{em}$ 578−700 nm) showed a 53% increase in Cy5 emission in the presence of $E_2$ (agonist) as compared to those of TOT (antagonist) and APO (no ligand), consistent with FRET due to the $E_2$-mediated ER-SRC1 interaction (Figure 6). There is no ER-SRC interaction without ligand (APO) or with the antagonist (TOT), which is known to disable the agonist-mediated ER-SRC interaction. The Cy5 emission intensity in the APO and TOT experiments is just the same as the sum of the background emission of $SiO_2$-TMR-NTA-$Ni^{2+}$ and control Cy5.

**$SiO_2$-TMR-NTA-$Ni^{2+}$-ERα SRC3 Interaction Experiments on Protein Microarrays.** A direct fluorometric assay and a FRET assay to demonstrate the ligand-regulated interaction between SRC and $SiO_2$-TMR-NTA-$Ni^{2+}$-ERα were performed on glass slides. The receptor interaction domain (RID) of the coactivator SRC3, with no fluorophore (for the fluorometric assay) and with a fluorescein label (for the FRET assay), was spotted on aldehyde slides and blocked remaining active sites on the array with bovine serum albumin (BSA). In both cases, $SiO_2$-TMR-NTA-$Ni^{2+}$-ERα was added in the presence of either an agonist ($E_2$), an antagonist ICI164,384 (ICI), or no ligand (APO).

In the fluorometric assay (Figure 7A), TMR was excited at 532 nm and emission monitored at 575 nm. As expected, recruitment of $SiO_2$-TMR-NTA-$Ni^{2+}$-ERα to the array surface through agonist−promoted receptor−coactivator interaction, evident from the strong 575 nm emission, occurred only in the

(28) Kim, S. H.; Tamrazi, A.; Carlson, K. E.; Daniels, J. R.; Lee, I. Y.; Katzenellenbogen, J. A. *J. Am. Chem. Soc.* **2004**, *126*, 4754−4755.
(29) Kim, S. H.; Tamrazi, A.; Carlson, K. E.; Katzenellenbogen, J. A. *Mol. Cell. Proteomics* **2005**, *4*, 267−277.

presence of $E_2$; essentially, no emission was observed with the antagonist ICI or no ligand (APO), indicating no interaction and minimal nonspecific binding under these conditions.

These interactions were confirmed by the FRET experiment (Figure 7B). In this case, the fluorescein-labeled SRC3-RID spotted on the array was excited at 490 nm, and TMR emission associated with the particle bound ERα was monitored at 580 nm. As before, strong emission was observed only in the presence of $E_2$, indicative of interaction and FRET; the very weak emission from the ICI and APO experiments comes from residual fluorescein emission in the TMR channel (i.e., at 580 nm), consistent with an absence of FRET.

## 4. Conclusion

In conclusion, we have described the preparation of dual-mode, silica-based TMR-doped, NTA-modified nanoparticles $SiO_2$-TMR-NTA-$Ni^{2+}$ (**1**) that through binding to His-tagged proteins enable a one-step protein isolation/purification (mode 1) and site-specific protein tagging with multiple fluorophores (mode 2). The well-defined particle properties, such as single-exponential decay of TMR under protein favorable environment, relative long life time, multiple TMR molecules unquenched by $Ni^{2+}$, high specificity, and capacity for oligo histidine tag of NTA, are essential for environment sensitive fluorometric and FRET assays with high sensitivity. Such dual-functional nanoparticles probe developed here can provide a new platform for simultaneous His-tagged protein purification and labeling that should prove to be widely useful in a variety of protein bioassay and interaction experiments. In addition, the data for nickel quenching obtained from lifetime measurements of $SiO_2$-TMR-NTA-$Ni^{2+}$ (**1**) provide useful information regarding the future design the nickel-binding fluorophore.

**Acknowledgment.** This work is supported by grants from the National Institutes of Health (5R37 DK15556) and the Siteman Cancer Center for Nanotechnology Excellence (SCCNE) at Washington University, through the University of Illinois Center for Nanoscale Science and Technology. We especially give thanks to Dr. Sung Chul Bae and Prof. Steve Granick for helping with fluorescence lifetime measurements and for discussion. XPS was carried out in the Center for Microanalysis of Materials, University of Illinois, which is partially supported by the U.S. Department of Energy under grant DEFG02-91-ER45439. We dedicate this paper to the memory of Nelson J. Leonard (1916−2006).

**Supporting Information Available:** Figures of IR spectra, TEM images, hydrodynamic diameters by dynamic light scattering, MALDI-TOF spectra, photograph of suspended nanoparticles, and XPS data for $SiO_2$-TMR and $SiO_2$-TMR-NTA-$Ni^{2+}$. This material is available free of charge via the Internet at http://pubs.acs.org.

JA074443F